Experimental and theoretical study of the npσ 1Σu+ (n≥4) N=0 excited states of D2: absolute absorption cross sections and branching ratios for ionization, dissociation and fluorescence

M. Glass-Maujean, A-M. Vasserot, Ch. Jungen, H. Schmoranzer, A. Knie, S. Kübler, A. Ehresmann

Experimental and theoretical study of the $np\sigma\ ^1\Sigma_u^+$ $(n \geq 4)$ $N = 0$ excited states of D_2: absolute absorption cross sections and branching ratios for ionization, dissociation and fluorescence

M. Glass-Maujean[1*], A-M. Vasserot[1], Ch. Jungen[2,3], H. Schmoranzer[4], A. Knie[5], S. Kübler[5] and A. Ehresmann[5]

[1] Laboratoire d'Etudes du Rayonnement et de la Matière en Astrophysique et Atmosphères, UMR 8112, Sorbonne Universités, UPMC Univ. Paris 06/Observatoire de Paris/CNRS F-75005, Paris, France

[2] Laboratoire Aimé Cotton du CNRS, Bâtiment 505 Université de Paris-Sud, F-91405 Orsay, France

[3] Department of Physics and Astronomy, University College London London WC1E 6BT, United Kingdom

[4] Fachbereich Physik, Technische Universität Kaiserslautern, D-67653 Kaiserslautern, Germany

[5] Institute of Physics and Center for Interdisciplinary Nanostructure Science and Technology (CINSaT), Heinrich-Plett-Str. 40, Universität Kassel, D-34132 Kassel, Germany

[*] corresponding author: M. Glass-Maujean

POSTAL ADDRESS: Laboratoire d'Etudes du Rayonnement et de la Matière en Astrophysique et Atmosphères, Université P. et M. Curie, 4, pl Jussieu, F-75252 Paris Cedex 05, France

phone number: +33(0)-1-4427-4326. e-mail: michele.glass@upmc.fr

January 7, 2016

Abstract

The absolute absorption cross sections for photoexcitation of D_2 to $N = 0$ Rydberg levels have been measured at a resolution of 0.001 nm in the 123500 - 135000 cm^{-1} spectral range. The experimental energies and line intensities are compared with *ab initio* multichannel quantum defect (MQDT) calculations of the $n \geq 4$ $np\sigma$ $^1\Sigma_u^+$ $N = 0$ levels of D_2. The calculations provide theoretical values of level positions, line intensities and autoionization widths. They are based on quantum-mechanical clamped-nuclei potential energy curves and dipole transition moments available for the lowest Rydberg members of the $np\sigma$ series. The overall agreement between experiment and theory is good. The decay dynamics of the excited $N = 0$ Rydberg levels is discussed based on the observed quantum yields for ionization, dissociation and fluorescence, and is compared with the yields previously observed in the analogous states of the H_2 isotopomer.

1 Graphical abstract

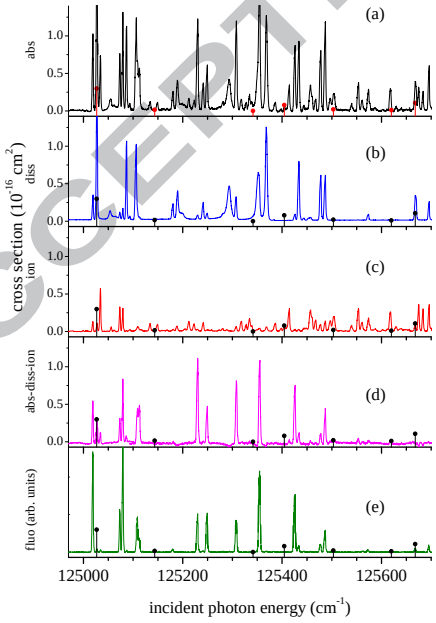

2 Highlights

- 46 photoabsorption transitions to $np\sigma\ ^1\Sigma_u^+$ $N = 0$ upper levels of D_2 measured and assigned.
- 14 previously unknown spectral lines observed and assigned.
- Absolute absorption line intensities, natural level widths and branching ratios for dissociation, ionization and fluorescence determined.
- Calculation from first principles of perturbed spectra in D_2.
- Quantitative agreement between observations and *ab initio* theory.

3 Introduction

This paper is the fourth in a series [1, 2, 3] dealing with the photoabsorption spectrum of molecular deuterium. This is a combined experimental and theoretical effort, in which multichannel quantum defect theory, MQDT, is used to interpret spectra taken at the SOLEIL and BESSY synchrotron radiation sources. The present paper is concerned with the $P(1)$ transitions leading to $N = 0$ excited states of $^1\Sigma_u^+$ symmetry recorded at BESSY, and specifically with their absorption intensities and decay dynamics.

The absorption spectrum of molecular deuterium has been recorded at room temperature using a 10 m normal-incidence monochromator at BESSY. The measured transition energies have an uncertainty of 1 cm^{-1}, which is less precise than the Fourier-transform (FT) measurements recorded at SOLEIL [3]. However, by using a monochromator, we are in a position to perform absolute intensity measurements and, by monitoring simultaneously the signals for dissociation, ionization and fluorescence, we also have access to the dissociation, ionization and fluorescence partial cross sections. The two techniques therefore complement each other. While most of the transitions observed here have been measured in the preceding paper, we report here, in addition to our study of the intensities and decay dynamics, a number of additional $P(1)$ transitions which had not been observed there.

4 Experiment

The experimental setup has been described in detail in previous papers [2, 4, 5, 6]. Briefly, the VUV photons coming from the undulator beamline U125/2-10m-NIM of BESSY II were dispersed by a 10 m normal-incidence

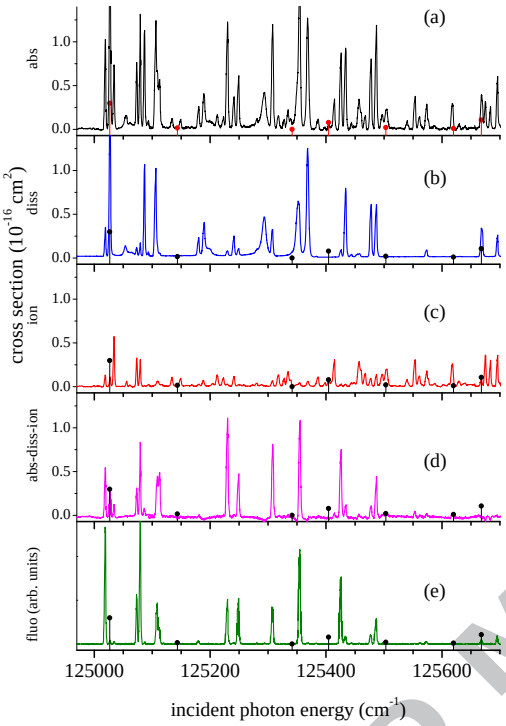

Figure 1:
(Color online) A section of the D_2 absorption and photoexcitation spectra recorded at BESSY. (a) (black online) absorption, σ_{abs}. (b) (blue online) dissociation, σ_{diss}. (c) (red online) ionization, σ_{ion}. (d) (violet online) $\sigma_{fluo} = \sigma_{abs} - \sigma_{diss} - \sigma_{ion}$, flurescence signal determined indirectly. (e) (green online) fluorescence measured directly. Calculated $P(1)$ transitions leading to $np\sigma, v, N = 0$ upper Rydberg levels are indicated by filled circles with intensities (on an arbitrary scale) corresponding to absorption.

monochromator equipped with a 4800-lines/mm grating giving an effective linewidth of 0.0010 nm (2 cm^{-1}) in first order [6]. This value represents the convolution of the apparatus function with the Doppler width at room temperature. The energy uncertainty is about ± 1 cm^{-1} and results mainly from a small residual non-linearity of the monochromator's energy scale (see [5]). The intensities of the absorption transitions, recorded at the effective resolution just mentioned, were calibrated directly, based on the known absorption path length (39 mm) and the gas pressure of 10 or 20 mTorr (13.3 or 26.7 μbar) at room temperature. Our experimental setup enables the excitation spectra for photoionization, photodissociation and visible molecular fluorescence to be recorded simultaneously. The photodissociation spectrum was recorded by monitoring the Ly$_\alpha$ emission, while the visible molecular fluo-

rescence was monitored in the 400-650 nm spectral range. The photoionization and photodissociation spectra were calibrated on the basis of absorption peaks that are known to be fully ionized or fully dissociated. The molecular fluorescence excitation cross section was obtained indirectly, by subtracting the photoionization and photodissociation cross sections from the photoabsorption cross section. These procedures are described and justified in detail in Ref. [5]. Fig. 1 displays a section of the experimental spectra obtained with the BESSY setup. Note how a given line may appear with very different intensities in the different detection channels. It is this information which allows the decay dynamics to be quantified.

5 Theory

The theoretical multichannel quantum defect approach used here reproduces step by step the approach described for H_2 in Ref. [7] and used in the preceding paper [3], with the only difference that the values of the reduced nuclear mass and the Rydberg constant have been adapted to the deuterium molecule. As previously the quantum defects and channel dipole transition moments were extracted from the highly accurate theoretical clamped-nuclei (Born-Oppenheimer) potential energy curves [8] and dipole transition moments [9], so that the input data for our calculations are fully *ab initio*.

The calculations were carried out in two steps. In a first set of computations all open ionization channels were omitted from the treatment and discrete energy level positions and Einstein spontaneous emission coefficients for the $P(1)$ transitions were evaluated and used for the analysis of the observed spectrum, cf. Fig. 1. In a second set of calculations all ionization channels, open and closed, were included and ionization profiles were evaluated, from which the autoionization widths were obtained. As in the preceding paper [3] we have omitted dissociation channels from our theoretical treatment.

6 Results

Spectra have been recorded in the wavelength range from 81.3 to 74.6 nm corresponding to 123000 - 134000 cm^{-1}. This range is roughly equivalent to the range from the ionization threshold to the third dissociation limit of diatomic deuterium. The results are summarized in Table 1. Many of the transitions listed in the Table have also been observed in the preceding paper [3]. The recommended values for the observed transition energies are those given in the preceding paper except for the values given in boldface

in the present Table 1 which are new. Before discussing the various aspects consecutively, we address the problem of determination of line positions, intensities and widths.

6.1 Determination of energies, intensities and widths

Each observed transition profile has been fitted to a Gaussian profile which yields the peak position, the peak area and peak width. The peak positions agree to within the uncertainty of the BESSY measurements with the more precise FT values from SOLEIL where these are available. A difficulty in determining line intensities, and particularly in applying Eq. (1) to the observed data, see Sec. 6.3 below, is that spectral lines are often blended. This difficulty may be overcome in many cases by exploiting the information obtained when several decay channels are monitored simultaneously. For instance, a spectral line may appear blended in one channel while appearing fully resolved in another, so that the number of unknown parameters in the fitting procedure of a given line profile can be kept to a minimum.

For each intensity determination, the uncertainty was taken as three times the statistical 1σ error, to which was added an estimated calibration uncertainty of 10% [2]. The width value obtained from each Gaussian fit represents the convolution of the Doppler width, the apparatus function and the natural width of the upper level of the transition. The de-convolution procedure applied to each profile in order to obtain the natural width is the same which we have used in the preceding paper [3]. The combined width of the Doppler broadening and the apparatus function amounts to 1.5 - 2.5 cm^{-1} depending on the experimental condition of each given run at BESSY. These values are of course larger than those observed in the FT study on SOLEIL, where the spectral resolution is higher and the temperature was lower. Nevertheless, where a comparison can be made, the natural widths extracted from the BESSY spectra are compatible with those obtained from the SOLEIL spectra. Fourteen new values could be added based on the BESSY measurements.

6.2 Energy levels

We have identified 46 $P(1)$ transitions. Out of these, 30 have already been listed in the preceding paper [3]. Three $P(1)$ transitions observed in the FT spectrum could not be resolved in the BESSY spectrum. These are $P(1)$ $9p\sigma, v = 4$, $8p\sigma, v = 5$ and $5p\sigma, v = 9$. On the other hand, 14 additional weak transitions could be detected in the BESSY spectra, since here the sensitivity is higher and the background noise lower, particularly in the ionization and

dissociation excitation spectra. These are: $10p\sigma$, $12p\sigma$ and $15p\sigma$ for $v = 0$, $9p\sigma$, $10p\sigma$ and $21p\sigma$ for $v = 1$, $11p\sigma$, $15p\sigma$ and $18p\sigma$ for $v = 2$, as well as $7p\sigma, v = 4$ and $v = 5$, $6p\sigma, v = 9$, and $4p\sigma$ and $5p\sigma$ $v = 12$. These newly identified transitions are printed in boldface in Table 1.

6.3 Line intensities

The peak area of each measured transition is related to the Einstein A coefficient for the same transition by

$$\int_p \sigma d\omega = \frac{1}{8\pi c\omega^2} A_{n,v,N\rightarrow X,v''=0,N''} \frac{2N+1}{2N''+1} n_{N''}, \qquad (1)$$

where $N'' = 1$ and $N = 0$ for the $P(1)$ transitions studied here. In Eq. (1), $\int_p$ is the integral of the measured absorption cross section σ over the given line profile p, $\omega = (E_{n,v,N} - E_{X,v''=0,N''})/hc$ is the incident photon energy in cm^{-1}, and $n_{N''}$ is the fraction of molecules in the rotational state N'' of the vibrational ground state at the given temperature of 300 K ($n_{N''} = 0.20$ in the present case). An experimental value for the Einstein coefficient for each transition is obtained from Eq. (1) by solving for A.

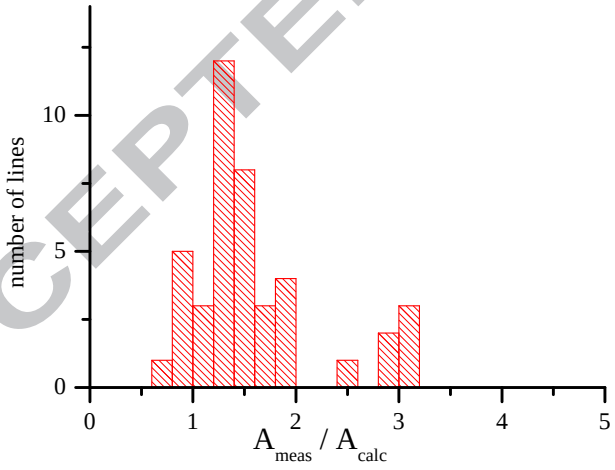

Figure 2:
Histogram of the ratios of the observed and calculated Einstein A coefficients of $P(1)$ transitions in D_2 absorption.

Table 1 and Fig. 2 compare the experimental Einstein A coefficients determined here for 42 $P(1)$ transitions with the values calculated theoretically

for transitions to $v'' = 0$. In the majority of cases the measured and calculated A values are in agreement with one another. However, in a number of instances the measured intensities turn out to be significantly larger than predicted by theory. This appears clearly from inspection of the statistical histogram of Fig. 2, and may in part be due to the uncertainty of our measurements. However, more likely, this arises from the fact that the spectral lines are overlapped. This hypothesis is corroborated by the fact that no calculated value has been found to be higher than the corresponding measured value including its error bar. Whenever a transition is blended by another transition which itself has been assigned, the corresponding value has been omitted from Table 1.

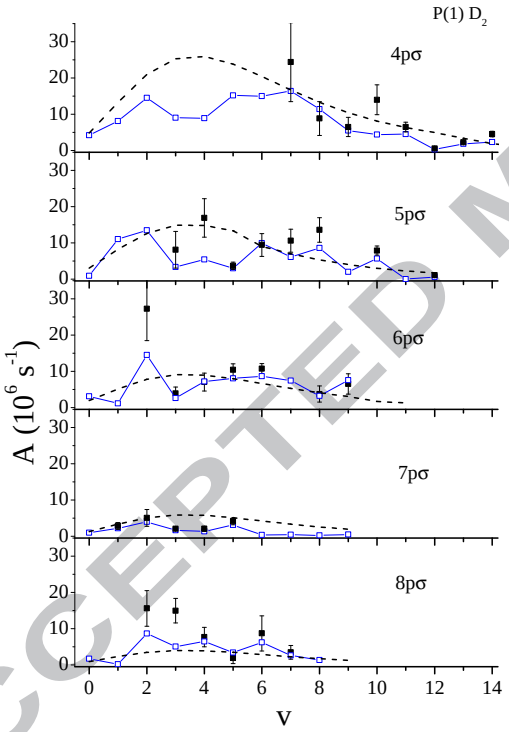

Figure 3:
(Color online) Einstein A coefficients for $P(1)$ absorption transitions in D_2 for the $np\sigma$, $n = 4 - 8$ states, plotted versus the vibrational quantum number v. Black squares with error bars: experimental values. Circles (blue online) connected by straight lines: MQDT calculation. Dashed lines: A values calculated using the Franck-Condon principle.

Fig. 3 provides a detailed comparison between the measured and calculated Einstein A coefficients for $v = 0 - 14$ and $n = 4 - 8$. The figure also in-

cludes the intensities expected in the situation where the Born-Oppenheimer approximation would hold and the Franck-Condon principle could be applied: the substantial deviations of the observed A values from those predicted in this approximation demonstrate the omnipresence of vibronic interactions. By contrast, the MQDT calculations are seen to correctly predict the irregular variations of the observed line intensities. Note that the vibronic interactions are far stronger in the $^1\Sigma_u^+$ upper states of the $P(1)$ transitions than in the $^1\Pi_u^-$ upper states of the $Q(1)$ transitions [2], a fact that has been known for a long time [10], and which is related to the different orientations of the $p\sigma$ and $p\pi$ orbitals with respect to the molecular frame. Fig. 3 shows that all of the $7p\sigma, v$ transitions are weakened by vibronic interaction, a *de facto* suppression of the $7p\sigma \leftarrow X$ electronic transition that causes the upper state to be difficult to be identified in the spectra.

Fig. 4 displays the observed and calculated Einstein A coefficients for higher $n-$ values, $n \geq 8$ up to $n \approx 28$, and for $v = 0$ to 3. Observed and calculated values are overall seen to be in fair agreement. A major discrepancy arises for $n = 11, v = 2$ where the observed intensity is three times larger than calculated. This transition appears well isolated in the spectrum, as no $P(N'')$, $Q(N'')$ or $R(N'')$ transition is predicted to be situated nearby.

6.4 Dynamical aspects

All excited levels studied in this work are situated above the second dissociation limit, D($1s$) + D($n = 2$), and are therefore subject to predissociation. The ionization threshold lies at 124715 cm^{-1}, so that below this threshold fluorescence and dissociation are the only accessible decay pathways. The radiative lifetimes of various rotational levels in the $4p\sigma, v = 0$ state are known to be 7.6 ± 0.6 ns [11], corresponding to a radiative width of $7 \cdot 10^{-4}$ cm^{-1}. According to the n^{-3} Rydberg scaling law we expect smaller radiative widths for the $np\sigma$ levels with $n \geq 5$. Our experimental data show that there is competition between the radiative and dissociative decay channels for most of the levels situated between 123500 and 124715 cm^{-1}, in the sense that the partial widths are comparable. We thus conclude that the dissociation widths of these levels must be $\leq 10^{-3}$ cm^{-1} as well. It may well be that the $4p\sigma, v = 5, N = 0$ level is fully dissociated, but since the corresponding $P(1)$ transition is blended, it is difficult to be certain.

For energies above 124715 cm^{-1} decay by autoionization also becomes energetically possible and is expected to take over eventually. We know that in H_2 none of the $np\sigma$ levels with $N = 0$ situated above the ionization threshold fluoresces [5]. However, vibrational autoionization is slower in the heavier isotopomer D_2 and, indeed, in the $5p\sigma, v = 4, N = 0$ level fluorescence

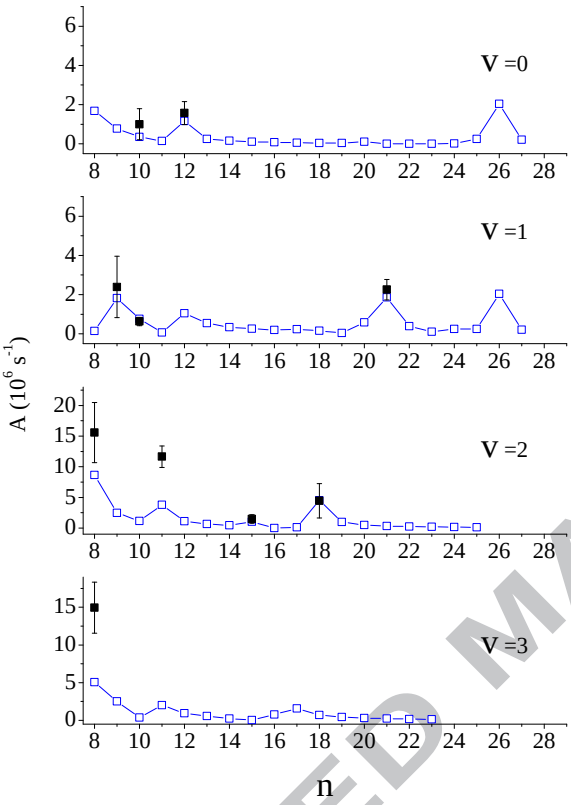

Figure 4:
(Color online) Einstein A coefficients for $P(1)$ absorption transitions in D_2 for the $np\sigma, v$, $v = 0 - 3$, levels plotted as functions of the principal quantum number n.

remains in the competition with a share of 17% of the total decay. The ionization and dissociation processes are particularly slow in this case. As in H_2, the $4p\sigma, v, N = 0$ levels are all fully dissociated in D_2. An exception occurs for $v = 10$ where an ionization yield of 27% is observed.

As already stated, ionization takes over completely in H_2 above the ionization threshold for $N = 0$, with the exception of the $4p\sigma$ levels which are dissociated. In D_2 dissociation subsists also in the $5p\sigma, v, N = 0$ manifold, with yields ranging from 0 to 100 %. Further, some of the $6p\sigma$ levels, $v = 2$ and 3, are also partially dissociated and the same is true even for $8p\sigma, v = 2, N = 0$. These observations, and particularly the differences between the decay dynamics in H_2 and D_2, are somewhat surprising as both, predissociation and autoionization, are non-adiabatic effects that are expected to be the weaker

the heavier the isotope. We shall come back to this point in Sec. 7 below.

6.5 Line widths

For fluorescence to be able to compete with dissociation and/or ionization, the predissociation and/or autoionization widths must be very small, i.e. $\ll 0.01$ cm^{-1}. For instance our calculation yields an ionization width of $3 \cdot 10^{-4}$ cm^{-1} for the $5p\sigma, v = 4, N = 0$ level, which is indeed of the same order as the radiative width. For all $N = 0$ levels where fluorescence has been observed, we find, as expected, that the measured width is far smaller than the experimental uncertainty.

For dissociation to be able to compete with ionization, the autoionization width must also be sufficiently small. For all $N = 0$ levels that appear in dissociation, the measured value of the width is smaller than its uncertainty, and the calculated autoionization width is ≤ 0.06 cm^{-1}. Moreover, the calculations predict ionization widths for the $4p\sigma, v, N = 0$ levels up to $v = 12$ that are smaller than 10^{-3} cm^{-1}. An exception is again the $v = 10$ level (cf. Sec. 6.4), for which we calculate an autoionization width as large as 0.03 cm^{-1}. The ionization yield observed in this case is 17 %, implying a dissociation partial width of ≈ 0.15 cm^{-1}, which again is too small to be detected in our experiment. Dissociation is particularly slow for this level, and in fact much slower than one could expect based on the previous study of H_2 [12].

Apart from the exceptions just discussed, the $np\sigma$ $N = 0$ levels of D_2 are found to be fully autoionized so that the experimental natural widths may be compared directly with the calculated autoionization widths. This is done in Fig. 5, which is seen to show good overall agreement of experiment and theory. Fig. 5 is a good example demonstrating the validity of the well-known $\Delta v = -1$ propensity rule for vibrational autoionization [10, 13, 14, 15]: the calculated and observed ionization widths shoot up by several orders of magnitude at the point where the $v^+ = v - 1$ threshold is passed, in other words, where the $v^+ = v - 1$ decay channel becomes accessible. After this spectacular onset, the widths decrease more or less smoothly as function of n, following the n^{-3} Rydberg scaling rule and in accordance with the two-channel autoionization formula given in Ref. [10]. This decrease is somewhat irregular due to local perturbations that affect the Rydberg series. For instance, $14p\sigma, v = 5, N = 0$ interacts with the perturber $5p\sigma, v = 9, N = 0$ which cannot autoionize via $\Delta v = -1$; the result is that the width of the perturbed level is reduced. This type of effect is of course accounted for by the multichannel treatment employed here.

For the purpose of comparison we have included in Fig. 5 the calculated

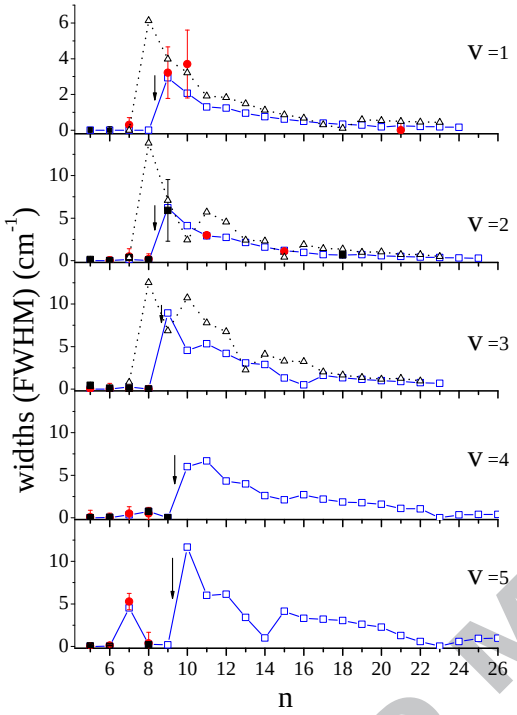

Figure 5:
(Color online) Upper state level widths for $P(1)$ transitions in D_2 absorption for $v = 1-5$, plotted versus the principal quantum number n. Filled circles with error bars (red online): experimental values (BESSY). Filled squares with error bars: experimental values (SOLEIL). Open squares connected by full lines (blue online): ionization widths calculated by MQDT. Open triangles connected by dotted lines: calculated widths of the same states in H_2. The vertical arrows indicate for each level v the position of the ionization limit $v^+ = v - 1$.

values from our previous study of $N = 0$ Rydberg levels in H_2 [7]. The $\Delta v = -1$ autoionization widths are known [2, 16] to scale according to $M^{-1/2}$ where M is the nuclear mass factor relevant for the process. Therefore the expectation is that the vibrational autoionization widths in H_2 should be by a factor 1.4 larger than in D_2. The maximum values shown in Fig. 5 correspond, very roughly, to a ratio of 2 for the first two series and to 1.3 for the third series. There is, therefore, qualitative albeit not exact agreement with the expectations based on the two-channel approximation.

7 Conclusion

Using a 10 m normal-incidence monochromator at BESSY we have measured the positions, intensities and widths of 42 $np\sigma\ ^1\Sigma_u^+, v, N = 0 \leftarrow X\ ^1\Sigma_g^+, v'' = 0, N'' = 1$ $P(1)$ transitions of D_2 between 123000 and 134000 cm^{-1}. The BESSY measurements are complementary to the preceding Fourier-transform study carried out at SOLEIL [3], as they provide absolute absorption cross sections as well as a wealth of information on the decay dynamics. Further, due to the higher sensitivity, 14 additional $P(1)$ transitions have been observed that had not been identified previously.

An interesting result concerns the decay dynamics and partial cross sections and their comparison with the analogous quantities in H_2. We have found that while ionization on the whole takes completely over in D_2 and in H_2 as expected when the excitation energy increases above the ionization threshold, dissociation and even fluorescence persist up to higher Rydberg members in D_2 than in H_2. This behavior is not intuitively understandable, since both autoionization and predissociation processes are expected to become slower when the nuclear mass increases. The higher density of levels present in D_2 as compared to H_2 is also an issue here, as it favors local interactions that become active when coincidences or near-coincidences occur between levels that may couple vibronically. In Ref. [2] we have presented a discussion of these effects in some detail, and come to the conclusion that the non-intuitive aspect of the differences between the D_2 and H_2 dynamics has genuine *multichannel* character and cannot be understood in the framework of simple models.

The role of level coincidences, leading to 'indirect' or 'accidental' predissociation or autoionization, has long been recognized in molecular physics [17]. In diatomic hydrogen it has been invoked to explain predissociation [18] and autoionization processes [19] that would not occur in a zero-order picture. The multichannel character of some of the observed phenomena which we discuss here may be regarded as a generalization of these earlier concepts. On the other hand, we have also found that some quantities, such as the $\Delta v = -1$ propensity-favored vibrational autoionization widths, do not deviate much from the expectations based on a two-channel model.

8 Acknowledgments

We acknowledge the Helmholtz-Zentrum Berlin - Electron storage ring BESSY II - for providing synchrotron radiation at the beamline U125/2-10m-NIM. In particular we would like to thank Gerd Reichardt and Andreas Balzer for their assistance with the experiments. The research leading to these results has received funding from the European Community's Seventh Framework Programme (FP7/2007-2013) under grant agreement No. 226716. A. K. would like to thank the Otto-Braun-Fonds of the University of Kassel for financial support. Ch. J. thanks the Miescher Foundation (Basel, Switzerland) for partial support.

References

[1] M. Glass-Maujean, Ch. Jungen, G. D. Dickenson, W. Ubachs, N. de Oliveira, D. Joyeux, and L. Nahon, J. Mol. Spectrosc. **315**, 147-154 (2015).

[2] M. Glass-Maujean, A.-M. Vasserot, Ch. Jungen, H. Schmoranzer, A. Knie, S. Kübler, and A. Ehresmann, J. Mol. Spectrosc. **315**, 155-171 (2015).

[3] M. Glass-Maujean, Ch. Jungen, G. D. Dickenson, W. Ubachs, N. de Oliveira, J. Mol. Spectrosc. (preceding paper).

[4] M. Glass-Maujean, Ch. Jungen, H. Schmoranzer, A. Knie, I. Haar, R. Hentges, W. Kielich, K. Jänkälä, and A. Ehresmann, Phys. Rev. Lett. **104**, 183002-1 - 183002-4 (2010).

[5] M. Glass-Maujean, Ch. Jungen, G. Reichardt, A. Balzer, H. Schmoranzer, A. Ehresmann, I. Haar, and P. Reiss, Phys. Rev. **A 82**, 062511-1 - 062511-13 (2010).

[6] G. Reichardt, J. Bahrdt, J.-S. Schmidt, W. Gudat, A. Ehresmann, R. Müller-Albrecht, H. Molter, H. Schmoranzer, M. Martins, N. Schwentner and S. Sasaki, Nucl. Instrum. Methods Phys. Res. Sect. A **467-468**, 462-465 (2001).

[7] M. Glass-Maujean, Ch. Jungen, H. Schmoranzer, I. Haar, A. Knie, P. Reiss, and A. Ehresmann, J. Chem. Phys. **135**, 144302-1 - 144302-12 (2011).

[8] G. Staszewska and L. Wolniewicz, J. Mol. Spectrosc. **212**, 208-212 (2002).

[9] L. Wolniewicz and G. Staszewska, J. Mol. Spectrosc. **217**, 181-185 (2003).

[10] G. Herzberg and Ch. Jungen, J. Mol. Spectrosc. **41**, 425-486 (1972).

[11] M. Glass-Maujean, J. Breton, B. Thieblemont, and K. Ito, J. Physique **45**, 1107-1111 (1984).

[12] M. Glass-Maujean, S. Klumpp, L. Werner, A. Ehresmann, and H. Schmoranzer, J. Chem. Phys. **126**, 144303-1 - 144303-8 (2007).

[13] R. S. Berry, J. Chem. Phys. **45**, 1228-1245 (1966).

[14] M. Raoult and Ch. Jungen, J. Chem. Phys. **74**, 3388-3399 (1981).

[15] Ch. Jungen and S. T. Pratt, Phys. Rev. Lett. **102**, 023201-1 - 023201-4 (2009).

[16] S. T. Pratt and Ch. Jungen, J. Chem. Phys. **137**, 174306-1 - 174306-6 (2012).

[17] G. Herzberg, in *Molecular Spectra and Molecular Structure, Vol. I* (van Nostrand Reinhold, New York, 1950).

[18] M. Glass-Maujean, J. Breton and P. M. Guyon, Phys. Rev. Lett. **40**, 181-184 (1978).

[19] Ch. Jungen and M. Raoult, Farad. Disc. Chem. Soc. **71**, 253-271 (1981).

[20] J. Liu, D. Sprecher, Ch. Jungen, W. Ubachs, and F. Merkt, J. Chem. Phys. **132**, 154301-1 - 154301-11 (2010).

Table 1: $P(1)$ transitions in the photoabsorption spectrum of the D_2 molecule

	v	$P(1)$ (obs) [a]	$obs-calc$	A_{calc} [b]	A_{obs}	Γ_{calc} [c]	Γ_{obs}	γ_{diss} [d]	γ_{ion}	γ_{fluo}
$10p\sigma$	0	**123572.6**[e,f]	**-0.4**	0.35	1.0 ± 0.8	0.00				
$11p\sigma$	0	123773.6		0.14	*	0.00				
$4p\sigma$	5	123891.7	0.4	15.15	*	0.00	0.1 ± 0.2	100 ± 5	0	0
$7p\sigma$	1	123901.7	0.0	2.18	2.8 ± 0.9	0.00	0.3 ± 0.4	56 ± 5	0	44 ± 5
$12p\sigma$	0	**123931.9**	**-0.3**	1.16	1.6 ± 0.6	0.00	**0.0 ± 0.3**	100 ± 3	0	0
$13p\sigma$	0	124046.1		0.25		0.00				
$14p\sigma$	0	124139.2		0.15		0.00				
$15p\sigma$	0	**124214.3**	**0.1**	0.11	*	0.00	**0.0 ± 0.3**			
$16p\sigma$	0	124275.5		0.077		0.00				
$5p\sigma$	3	124326.4	0.6	3.33	8.1 ± 5.1	0.00	0.0 ± 0.3	31 ± 4	0	69 ± 4
$17p\sigma$	0	124368.6		0.06		0.00				
$18p\sigma$	0	124404.3		0.05		0.00				
$19p\sigma$	0	124434.7		0.04		0.00				
$20p\sigma$	0	124459.7		0.10		0.00				
$8p\sigma$	1	124468.1		0.14		0.00				
$21p\sigma$	0	124484.7		0.000		0.00				
$22p\sigma$	0	124504.2		0.001		0.00				
$23p\sigma$	0	124521.4		0.000		0.00				
$24p\sigma$	0	124550.2		0.02		0.00				
$25p\sigma$	0	124562.1		0.25		0.00				
$6p\sigma$	2	124569.0	-0.9	14.52	27 ± 9	0.00	0.0 ± 0.1	36 ± 6	0	64 ± 6
$26p\sigma$	0	124573.5		2.03		0.00				
$27p\sigma$	0	124582.8		0.20		0.00				
$9p\sigma$	1	**124870.0**	**-0.5**	1.82	2.4 ± 1.6	2.93	**3.2 ± 1.4**	0	100 ± 2	0
$4p\sigma$	6	125026.7	0.0	15.02	*	2.0E-06				
$10p\sigma$	1	**125143.5**	**0.0**	0.76	0.6 ± 0.2	2.06	**3.7 ± 1.9**	0	100 ± 2	0
$11p\sigma$	1	125341.4		0.06		1.29				
$7p\sigma$	2	125404.5	0.0	3.96	5.1 ± 2.3	0.17	0.5 ± 0.9	0	100 ± 2	0
$12p\sigma$	1	125503.1		1.04		1.23				
$13p\sigma$	1	125620.1		0.55		0.95				
$5p\sigma$	4	125667.6	-0.3	5.44	16.9 ± 2.3	2.9E-04	0.1 ± 0.8	69 ± 3	15 ± 1	16 ± 1
$14p\sigma$	1	125713.4		0.34		0.76				
$15p\sigma$	1	125788.6		0.26		0.61				
$16p\sigma$	1	125850.0		0.20		0.49				
$17p\sigma$	1	125900.5		0.23		0.39				
$6p\sigma$	3	125931.3	0.1	2.63	3.9 ± 1.8	3.0E-03	0.0 ± 0.4	24 ± 6	76 ± 6	0
$18p\sigma$	1	125944.9		0.15		0.33				
$19p\sigma$	1	125979.6		0.04		0.28				
$20p\sigma$	1	126009.2		0.58		0.19				
$8p\sigma$	2	126025.2	-0.3	8.64	15.6 ± 4.9	0.013	0.2 ± 0.6	6 ± 2	94 ± 2	0
$21p\sigma$	1	**126039.0**	**0.3**	1.86	2.3 ± 0.5	0.24	**0.0 ± 0.4**	0	100 ± 5	0
$22p\sigma$	1	126060.3		0.39		0.21				
$23p\sigma$	1	126079.9		0.11		0.18				
$4p\sigma$	7	126087.3	0.1	16.40	24 ± 11	3.8E-04	0.0 ± 0.4	100 ± 2	0	0
$24p\sigma$	1	126097.2		0.25		0.15				
$9p\sigma$	2	126374.7		2.48		6.20				
$10p\sigma$	2	126647.7		1.16		4.10				
$7p\sigma$	3	126816.6	-0.1	1.65	2.1 ± 0.7	0.27	0.0 ± 0.5	0	100 ± 5	0
$11p\sigma$	2	**126870.5**	**1.7**	3.77	11.6 ± 1.8	2.91	**3.0 ± 0.3**	0	100 ± 5	0
$5p\sigma$	5	126937.2	-0.4	3.00	3.7 ± 1.0	1.4E-03	0.0 ± 0.3	100 ± 5	0	0
$12p\sigma$	2	127011.0		1.12		2.74				
$4p\sigma$	8	127071.4	-0.5	11.42	8.8 ± 4.7	2.5E-04	0.0 ± 0.6	100 ± 5	0	0
$13p\sigma$	2	127128.9		0.64		2.14				
$14p\sigma$	2	127222.5		0.46		1.60				
$15p\sigma$	2	**127298.1**	**0.7**	1.01	1.5 ± 0.7	1.21	**1.1 ± 0.2**	0	100 ± 5	0
$6p\sigma$	4	127310.9	0.1	7.21	7.0 ± 2.5	0.032	0.0 ± 0.5	0	100 ± 5	0
$16p\sigma$	2	127359.6		0.002		0.97				
$17p\sigma$	2	127409.4		0.12		0.70				

Table 1 (continued)

	v	$P(1)$ (obs) [a]	$obs-calc$	A_{calc} [b]	A_{obs}	Γ_{calc} [c]	Γ_{obs}	γ_{diss} [d]	γ_{ion}	γ_{fluo}
$8p\sigma$	3	127444.1	0.8	5.08	14.9 ± 3.4	0.01	0.0 ± 0.4	0	100 ± 5	0
$18p\sigma$	2	**127460.4**	**-0.2**	4.51	4.4 ± 2.8	0.68	**0 ± 0.6**	**0**	**100 ± 5**	**0**
$19p\sigma$	2	127492.1		0.98		0.70				
$20p\sigma$	2	127522.0		0.48		0.59				
$21p\sigma$	2	127548.1		0.32		0.50				
$22p\sigma$	2	127570.8		0.23		0.42				
$23p\sigma$	2	127590.7		0.18		0.37				
$24p\sigma$	2	127608.1		0.14		0.33				
$25p\sigma$	2	127623.4		0.12		0.29				
$9p\sigma$	3	127814.6		2.51		8.93				
$4p\sigma$	9	127969.1	-0.2	5.45	6.5 ± 2.7	7.5E-05	0.0 ± 0.3	100 ± 5	0	0
$10p\sigma$	3	128084.7		0.35		4.55				
$5p\sigma$	6	128153.7	0.3	9.96	9.4 ± 3.1	0.084	0.1 ± 0.3	0	100 ± 5	0
$7p\sigma$	4	**128197.4**	**0.4**	1.35	2.0 ± 0.7	0.34	**0.5 ± 0.8**	0	100 ± 5	0
$11p\sigma$	3	128305.9		2.01		5.34				
$12p\sigma$	3	128455.5		0.96		4.19				
$13p\sigma$	3	128574.1		0.56		3.08				
$6p\sigma$	5	128616.7	0.0	8.06	10.4 ± 1.7	0.045	0.0 ± 0.3	0	100 ± 5	0
$14p\sigma$	3	128667.9		0.24		2.88				
$15p\sigma$	3	128742.7		0.02		1.30				
$16p\sigma$	3	128798.8		0.78		0.51				
$4p\sigma$	10	128813.6	-0.6	4.64	14.0 ± 4.1	0.031	0.3 ± 0.3	73 ± 7	27 ± 7	0
$8p\sigma$	4	128825.5	0.7	6.44	7.7 ± 2.7	0.73	0.5 ± 0.7	0	100 ± 5	0
$17p\sigma$	3	128862.2		1.56		1.61				
$18p\sigma$	3	128903.1		0.70		1.34				
$19p\sigma$	3	128938.7		0.44		1.15				
$20p\sigma$	3	128969.3		0.30		1.00				
$21p\sigma$	3	128995.6		0.24		0.88				
$22p\sigma$	3	129018.5		0.18		0.77				
$23p\sigma$	3	129038.4		0.15		0.69				
$9p\sigma$	4	129191.8		1.48		0.03				
$5p\sigma$	7	129290.5	0.9	6.12	10.6 ± 3.2	0.057	0.0 ± 0.4	23 ± 4	77 ± 4	0
$10p\sigma$	4	129445.6		0.02		6.00				
$7p\sigma$	5	**129518.**4	**-0.1**	3.07	4.1 ± 0.9	4.53	**5.3 ± 1.0**	0	100 ± 5	0
$4p\sigma$	11	129596.3	-0.6	4.49	6.5 ± 1.3	5.3E-04	0.0 ± 0.4	100 ± 5	0	0
$11p\sigma$	4	129685.5		1.27		6.67				
$12p\sigma$	4	129837.1		0.14		4.32				
$6p\sigma$	6	129861.7	-0.9	8.67	10.7 ± 1.5	0.65	0.6 ± 0.3	0	100 ± 5	0
$13p\sigma$	4	129956.7		0.47		3.98				
$14p\sigma$	4	130049.3		0.04		2.60				
$8p\sigma$	5	130112.8	-0.5	1.38	1.9 ± 1.5	0.28	0.4 ± 1.3	0	100 ± 5	0
$15p\sigma$	4	130145.3		3.41		2.11				
$16p\sigma$	4	130196.3		1.17		2.72				
$17p\sigma$	4	130245.9		0.62		2.19				
$18p\sigma$	4	130288.2		0.41		1.85				
$4p\sigma$	12	**130308.6**	**1.4**	0.29	0.6 ± 0.1	9.7E-04	**0.0 ± 0.4**	100 ± 5	0	0
$19p\sigma$	4	130324.2		0.26		1.77				
$20p\sigma$	4	130354.9		0.18		1.58				
$5p\sigma$	8	130377.0	-0.5	8.59	13.6 ± 3.4	1.6E-03	0.1 ± 0.2	100 ± 5	0	0
$21p\sigma$	4	130381.4		0.26		1.10				

Table 1 (continued)

	v	$P(1)$ (obs) [a]	$obs-calc$	A_{calc} [b]	A_{obs}	Γ_{calc} [c]	Γ_{obs}	γ_{diss} [d]	γ_{ion}	γ_{fluo}
$22p\sigma$	4	130404.2		0.12		1.04				
$29p\sigma$	4	130500.5		0.40		0.00				
$9p\sigma$	5	130507.6		0.56		0.18				
$30p\sigma$	4	130514.9		0.41		0.36				
$31p\sigma$	4	130522.1		0.28		0.40				
$32p\sigma$	4	130529.0		0.20		0.39				
$33p\sigma$	4	130535.4		0.15		0.30				
$34p\sigma$	4	130541.2		0.12		0.28				
$7p\sigma$	6	130707.2		0.34		0.25				
$10p\sigma$	5	130811.8		1.79		11.65				
$4p\sigma$	13	130991.6	0.2	1.37	2.2 ± 0.4	3.1E-03	0.2 ± 0.3	100 ± 5	0	0
$11p\sigma$	5	131002.7		0.06		6.00				
$6p\sigma$	7	131050.0	0.1	7.41	*	1.98				
$12p\sigma$	5	131159.3		0.82		6.13				
$13p\sigma$	5	131276.4		0.17		3.41				
$14p\sigma$	5	131352.0		0.000		1.00				
$5p\sigma$	9	131375.2		1.99		1.51				
$8p\sigma$	6	131403.1	-0.6	6.18	8.7 ± 4.8	2.06	2.2 ± 1.2	0	100 ± 5	0
$15p\sigma$	5	131460.2		1.53		4.12				
$16p\sigma$	5	131519.7		0.69		3.31				
$17p\sigma$	5	131570.2		0.44		3.20				
$4p\sigma$	14	131590.3	5.2	2.55	4.5 ± 0.7	2.6E-04	0.0 ± 0.3	100 ± 5	0	0
$18p\sigma$	5	131612.9		0.28		3.04				
$19p\sigma$	5	131648.9		0.18		2.60				
$20p\sigma$	5	131679.6		0.10		2.28				
$21p\sigma$	5	131705.6		0.04		1.27				
$22p\sigma$	5	131727.2		0.001		0.57				
$23p\sigma$	5	131743.5		0.23		0.03				
$9p\sigma$	6	131756.1		0.49		0.03				
$24p\sigma$	5	131770.6		0.33		0.57				
$25p\sigma$	5	131785.1		0.22		0.95				
$26p\sigma$	5	131798.3		0.16		0.96				
$38p\sigma$	5	131885.6		0.21		0.82				
$7p\sigma$	7	131887.5		0.40		0.00				
$39p\sigma$	5	131890.8		0.12		0.41				
$10p\sigma$	6	132058.9		0.49		12.00				
$6p\sigma$	8	132168.0	-0.3	3.25	3.7 ± 2.2	1.28	0.9 ± 0.9	0	100 ± 5	0
$11p\sigma$	6	132267.3		0.95		19.47				
$5p\sigma$	10	132336.9	2.9	5.66	7.9 ± 1.3	0.30	0.3 ± 0.2	0	100 ± 5	0
$8p\sigma$	7	132582.6	-0.7	2.61	3.5 ± 1.9	2.52	1.8 ± 1.0	0	100 ± 5	0
$5p\sigma$	11	133159.1		0.01		0.12				
$6p\sigma$	9	**133324.6**	**-1.0**	7.56	6.5 ± 2.8	7.07	**7.5 ± 1.0**	0	100 ± 5	0
$5p\sigma$	12	**134028.7**	**8.4**	0.63	1.1 ± 0.5	0.062	**0.0 ± 0.3**	100 ± 5	0	0

[a] ν/c, observed transition energy in cm^{-1}. When no entry $obs-calc$ is given, the transition has not been observed and the energy given corresponds to the calculated value.

[b] A, emission probability for the transition to $X^1\Sigma_g^+, v''=0, N''=1$, in 10^6 s^{-1}.

[c] Γ/hc, level width (FWHM) in cm^{-1}. The calculated widths are ionization partial widths.

[d] γ, experimental decay branching ratio in %.

[e] The positions of the upper state energy levels above the $v''=0, N''=0$ ground state level are obtained by adding the ground-state rotational energy 59.78 cm^{-1} ($N''=1$) [20] to the transition energy.

[f] Transition energies in boldface correspond to new assignments. The recommended values for the observed transition energies are those of the preceding paper except for the entries in boldface which are new.

* blended line.